Investigaciones Geográficas • Instituto de Geografía • UNAM
eISSN: 2448-7279 • DOI: dx.doi.org/10.14350/rig.60394 • ARTICLES
Num. 107 • April • 2022 • e60394
www.investigacionesgeograficas.unam.mx

Does land-use affect the temperature distribution across the city of Tuxtla Gutiérrez, Chiapas, México?

¿El uso de suelo afecta la distribución de temperatura en la ciudad de Tuxtla Gutiérrez, Chiapas, México?

Itzel Castro-Mendoza,* José René Valdez-Lazalde,** Geoffrey Donovan,*** Tomás Martínez-Trinidad,** Francisca Ofelia Plascencia-Escalante,** Williams Vázquez-Morales****

Received: 28/05/2021. Approved: 6/02/2022. Published: 18/02/2022

Abstract. A combination of natural (tropical latitudes) and human induced (Climate Change, Urban heat island) conditions give rise and exacerbate extreme hot temperatures, but mechanisms are unclear. Land use and land cover change (LULC) is considered one of the main causes of Urban Heat Island (UHI) but its contribution varies depending on local conditions. This study focuses on determining the influence of land use change on the UHI effect in Tuxtla Gutiérrez City by investigating the relationship between LULC and land surface temperature (LST). Through Landsat 5 and Landsat 8 imagery, this study analyzes historical LST. In 2017, the highest LST (>40 °C) occurred in the metal ceiling land class, which is made up of malls with open-air parking zones. This coverage occupied less than 3% of the total city area. Bare agriculture soil (BAS) class, located mainly on the periphery of the city, represented 11% of the city, and reported a mean LST of 35 °C, followed by asphalt roads with 34 °C and concrete ceiling with 32 °C. The lowest LST (< 28 °C), occurred in contiguous areas of trees greater than 3 ha. The LST variation when land use changed from trees to another coverage (1.3 to 3.1 °C) is higher than in the opposite direction (0.1 to 1.2 °C). The elimination or replacement of tress with impervious surfaces are the main causes for LST increase in Tuxtla Gutiérrez.

Keywords: Land use and land cover change, Land surface temperature, Urban heat island.

Resumen. La combinación de condiciones naturales (latitudes tropicales) y antropogénicas (Cambio Climático, Isla de Calor Urbana) inducen el incremento extremo de la temperatura; aunque los mecanismos no son claros. El cambio de uso de suelo es una de las principales causas de la Isla de Calor Urbana (ICU), aunque su intensidad depende de las condiciones locales. La investigación del medio ambiente en entornos urbanos es de relevancia, considerando que para el año 2030 el 60% de la población mundial se concentrará en ciudades y desde ahí enfrentará condiciones climáticas cada vez más extremas. Este estudio se centra en la relación del cambio de uso de suelo y la temperatura de

* Instituto Nacional de Investigaciones Forestales, Agrícolas y Pecuarias, Campo Experimental Centro Chiapas, Carretera Ocozocoautla-Cintalapa km 3, 9140, Ocozocoautla de Espinosa, Chiapas, México. ORCID: https://orcid.org/0000-0002-5356-9829. Email: castro.itzel@inifap.gob.mx. Autor de correspondencia.
** Colegio de Postgraduados, Campus Montecillo, Posgrado en Ciencias Forestales, Km. 36.5 Carretera México-Texcoco, 56230, Montecillo, Texcoco, Estado de México, México. Email: valdez@colpos.mx, tomtz@colpos.mx, fplascen@colpos.mx
*** USDA Forest Service, PNW Research Station, 620 SW Main, Suite 400 Portland, Estados Unidos de América. Email: geoffrey.donovan@usda.gov
**** Universidad de Ciencias y Artes de Chiapas, Programa de Gestión de Riesgos y Cambio Climático, Libramiento Norte Poniente No. 1150, edificio 21, Ciudad Universitaria, colonia Lajas Maciel, 29039, Tuxtla Gutiérrez, Chiapas, México. Email: williams.vazquez@unicach.mx

superficie (TS) para conocer su influencia en la ICU de la ciudad de Tuxtla Gutiérrez.

A fin de conocer el patrón espacial de las temperaturas extremas en la ciudad de Tuxtla Gutiérrez, Chiapas se analizó el comportamiento histórico de la temperatura del aire (TA) y de superficie (TS). Respecto a la TA, a partir de 1980 la frecuencia de las temperaturas superiores a 40 °C aumentó en un 18% y de las temperaturas nocturnas por arriba de los 28 °C en un 14%. El análisis histórico de temperaturas ambientales ayudó a determinar las tres fechas para la obtención de imágenes Landsat 5 (5 de abril de 2001) y Landsat 8 (1 de abril de 2011 y 2017). Para el análisis termal se emplea el Método de Clasificación de Emisividad el cual estima las TS con base en la emisividad reportada para cada uso y cobertura de suelo; en este estudio se emplean nueve clases: agua, árbol, camino de asfalto, césped, suelo desnudo, suelo agrícola desnudo, techo de concreto, techo de metal y techo de teja.

En 2017, la máxima TS (>40 °C) se registró en los techos de metal de centros comerciales con estacionamientos a cielo abierto. Este uso de suelo cubre menos del 3% de la ciudad. El suelo desnudo agrícola cubre la periferia de la ciudad y representa el 11% de la ciudad, se reporta con una TS promedio de 35 °C, seguida de los caminos de asfalto con 34 °C y techos de concreto con 32 °C. La resolución espacial de las imágenes limita la apreciación del efecto amortiguador de temperaturas de un árbol y únicamente es sensible al efecto de agrupaciones, por ello la mínima TS (< 28 °C) se registra en zonas arboladas mayores a 3 ha. La variación de TS cuando se elimina la cobertura arbórea (1.3 a 3.1 °C) es mayor que cuando se reforesta (0.1 a 1.2 °C). Se recomienda realizar el análisis con imágenes termales de mayor resolución espacial para apreciar el efecto refrescante de árboles individuales.

Comparando los resultados entre las tres fechas de análisis, la cobertura que más ha disminuido en superficie es árbol convirtiéndose en suelo agrícola desnudo, techo de concreto y teja. Estos cambios de cobertura se asocian al aumento en la temperatura promedio de la ciudad, que en el año 2001 se encontraba en el rango de temperatura poco agradable (29° a 31°C), para 2011 era extremadamente desagradable (31° a 33 °C) y en 2017 llego al rango de temperatura de condiciones de estrés (33° a 35 °C).

El reemplazo de árboles por superficies impermeables es la principal causa del aumento de la TS en Tuxtla Gutiérrez. La metodología empleada permite el registro de temperatura de superficie de las diferentes coberturas dentro de la ciudad, evitando la homogenización del terreno como se haría con una metodología basada en NDVI. Sin embargo, un área de oportunidad para mejorar los resultados obtenidos con esta metodología es la medición directa de la emisividad de superficie, así como el registro termal durante la noche.

Palabras clave: Cambio de uso de suelo, isla de calor urbana, Landsat, temperatura de superficie, temperatura del aire.

INTRODUCTION

Human activities change weather patterns at global and local scales (IPCC, 2018), causing cities experience consistently higher temperatures than surrounding rural areas (Oke, 1982; Howard, 1988; Eniolu *et al.*, 2013). The Urban Heat Island (UHI) effect is a pressing policy issue, because of climate change, and that 60% of the world´s population is forecast to live in urban areas by 2030 (UN, 2018).

In Mexico, since 1990, urbanization has rapidly grown in tropical latitudes (Reyes and López, 2011). These trends of tropical urbanization and rising temperatures are seen in Tuxtla Gutiérrez (TGZ), which is the second most populated city of the Mexican tropics and home to 10% of the population of the state of Chiapas.

In the last three decades, temperatures in TGZ have risen in the dry season (De la Mora et al., 2016). However, there is little information about how much urbanization has contributed to rising temperatures and UHI impacts, people´s wellbeing, economy and public health (Coello, 2015; Díaz-Nigenda *et al.*, 2018; López-Pérez *et al.*, 2019)we show a thermal comfort field study and adaptive thermal comfort model in educational buildings under tropical Aw climate, considering air conditioning systems (AC. Therefore, we examine the relationship between land-use change and extreme temperatures in TGZ.

UHI results from thermal equilibrium between atmospheric temperature (AT) and land cover with different land surface temperature (LST) (Oke, 1982). UHI intensity depends on the albedo and thermal inertia of construction materials, building density, aspect ratio, sky view factor (SVF), industrial development, traffic congestion, cloud cover, wind speed, precipitation, city geometry, and relative humidity. However, the main diver of UHI is land-use change (Li *et al.*, 2018), a factor that explains about 70% of the total variance in land surface temperature (LST) (Oke, 1973; Imhoff *et al.*, 2010)town or city (as measured by its population.

Recently, remote sensing data have helped UHI research by providing low-cost LST data at

adequate temporal frequency (Sobrino *et al.*, 2004; Amanollahi *et al.*, 2016; Avdan and Jovanovska, 2016)three methods to retrieve the land surface temperature (LST. Sensors such as MODIS (Moderate Resolution Imaging Spectroradiometer) and AVHRR (Advanced Very High Resolution Radiometer), offer thermal infrared information suitable for regional studies due to their spatial scale and spectral resolution (Mas, 2011; Amanollahi et al., 2016). Landsat imagery has been widely used at a finer scale for research (Zhao-Liang, Bo-Hui, *et al.*, 2013; Chen *et al.*, 2017; Tan *et al.*, 2017)based on a number of data used to build 2.5 D model; land cover, land use, geometrical factors and shadow layers. The raw air temperature measurements were filtered, georeferenced and interpolated to create maps of temperature variations. The expected influencing parameters on the development of the UHI were derived and prepared for regression modelling. The results showed that the difference in temperature across Birmingham city through two years of ground measurements (June 2012–June 2014.

LST requires information on radiance and emissivity which can be measured in situ or by remote sensing (Sobrino *et al.*, 2004, 2008; Cook *et al.*, 2014; Jeevalakshmi *et al.*, 2017; Tan *et al.*, 2017)which retrieves epsiv only from TIR data and (2. Landsat 4, 5, and 7 images have one thermal band and Landsat 8 has two. Before Landsat 8, NASA and the United States Geological Services worked to develop LST products based on the thermal archive data of Landsat missions (Cook *et al.*, 2014). For the purpose, they automated two methods: a) Single channel technique for imagery with one thermal band, and b) Multichannel technique (Split window) for Landsat 8 (Weng *et al.*, 2004; Sobrino *et al.*, 2008; Tan *et al.*, 2017) urban land use/land cover, geo-/biophysical and also a key input for climate models. LANDSAT 8, the latest satellite from LANDSAT series, has given lot of possibilities to study the land processes using remote sensing. In this study an attempt has been made to estimate LST over Chittoor district, Andhra Pradesh, India, using LANDSAT 8 – Operational Line Imager & Thermal Infrared Sensor (OLI & TIRS. The accuracy of both methods depends on the atmospheric profile information available for the scene location and scene capture time (Zhao-Liang, Hua, *et al.*, 2013; Cook *et al.*, 2014) especially for the emissivity retrieval.

Surface emissivity is a measure of the energy emitted as thermal radiation from a given land coverage (Sobrino *et al.*, 2012). When measured with a remote sensor, it varies with geometry, surface materials, surface roughness, ground humidity, view angle, and atmospheric information such as relative humidity, wind speed, cloud cover and precipitation (Kahle, 1987; Suomi, 2014; Ermida *et al.*, 2017; Gulbe *et al.*, 2017)but obtained with different viewing angles, to calibrate a simple model capable of characterizing the LST angular variability. The exercise is performed using MODIS (Aqua and Terra. In absence of atmospheric information, researchers can use other methods for surface emissivity retrieval. The most common method is the Normalized Difference Vegetation Index threshold method, $NDVI^{THM}$ (Sobrino *et al.*, 2008), which assigns an emissivity value to a given land coverage, bare soil or full vegetation, according to estimated NDVI values. However, $NDVI^{THM}$ has limitations; surfaces such as asphalt, or other common materials in urban environments, can cause inaccurate estimations of LST (Sobrino *et al.*, 2008). A more accurate method than $NDVI^{THM}$ for urban areas is the Emissivity Classification Method (ECM), which assigns emissivity values to each land cover-land use class, based on the ASTER spectral library (ASL, https://speclib.jpl.nasa.gov/) reported by Sobrino *et al.,* 2012.

In this research we examined the relationship between LULC and extreme temperatures in TGZ. Fist we estimated the surface UHI for the city of TGZ for three years (2001, 2011, and 2017) from historical analysis of air temperature. Later, we used Landsat 5 (TM) and 8 (OLI) imagery to define land use/land cover. Based on the cover types we retrieved LST by ECM method, as emissivity data were not available for the study area.

CHARACTERIZATION OF THE AREA

The city of Tuxtla Gutiérrez (TGZ) is the capital of Chiapas, a state located in southeastern Mexi-

co between 16º 48' 46" N, 93° 13' 12" O and 16° 40' 49" N, 93 ° 02' 19" O coordinates (Figure 1). Elevation ranges from 435 m to 917 m (Figure 1). The climate is warm and sub-humid with an average annual rainfall of 915 mm the majority of which falls in the summer (INEGI, 2017). The historical records registered 19 days with temperatures above 30 °C and 25.7 days of dry conditions per year with a mean annual temperature of 25.4ºC. The hottest month is April with a mean maximum historical temperature of 45.5ºC. The city of TGZ occupies a valley surrounded on the south by Mactumatzá Hill and on the east by The Sumidero Canyon National Park; both barriers hinder air flow and influence winds from the northwest with an average speed of 9.7 km/hr, reaching gusts during winter of 36 km/hr (Díaz-Nigenda *et al*., 2018).

The Sabinal River crosses the city through The Sumidero Canyon National Park to the Grijalva River. The predominant types of soil are Leptosols, Regosols, Luvisol and Vertisols. The city is surrounded by 4.9 km of Natural Protected and Conservation Areas of low deciduous forest (ICIPLAM, 2013). Almost 75% of the urban flora is exotic (Román, 2017) and distributed among 193 parks and a country club (ICIPLAM, 2015).

The city, as the main economic center of the state, had a population of 537,102, in 2010, which is an increase of 10% from 2005 (INEGI, 2013; CEIEG, 2014) and between 2007 and 2018 it grew in area from 7.8 km^2 to 107 km^2 (HATG, 2007), an increase of 11% annually. Since 1986, residential development has an annual increase of 3% in TGZ (Silva *et al*., 2015). The Municipal Citizen Planning Institute (ICIPLAM) of TGZ

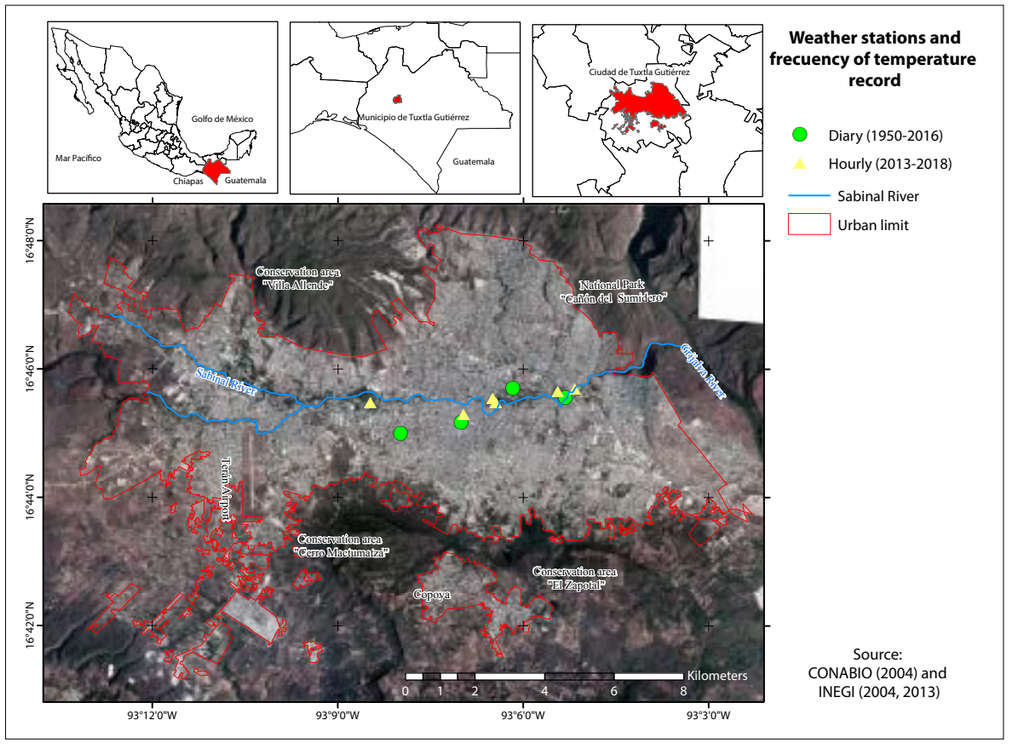

Figure. 1. Location of weather stations in the city of Tuxtla Gutiérrez, Chiapas, Mexico.

has identified an irregular land use-land cover (LULC) change in the city since the 1980s, one that limits urban planning and interfere with the implementation of green areas as part of urban developments (ICIPLAM, 2013) since vegetation competes with housing space.

MATERIALS AND METHODS

Data

We analyzed air temperature data from 11 weather stations (Figure 1) with a daily (1951-2016) and hourly (2013-2018) record. We used these data as reference to choose the capture date of the Landsat scenes downloaded and not for the analysis of UHI in TGZ because weather stations are not evenly distributed across the city. Classification of LULC were validated in ground and with a high spatial resolution image (0.5 m) and a mosaic of orthophotos. Ground truthing of LST retrieved from Landsat images (Table I and II) was done at ten verification sites in 2019, May 29th and 30th using an Extech IR201A infrared thermometer with adjustable emissivity between 15:00 and 17:00 hrs. All images were processed on ArcMap 10.5 package.

Methodology

We were interested in the impact of extreme temperatures on human wellbeing and comfort. Therefore, we used vulnerability levels due to extreme air

Table I. Data used for land surface temperature (LST) retrieve at Tuxtla Gutiérrez City.

Variable	Instrument	Source	Space scale	Time scale
Daily air temperature	Four weather stations	Weather National Service	N/A	1951 to 2016
Hourly air temperature	One weather station	Electricity Federal Commission	N/A	2013 to 2016
	Five weather stations	Weather net of the Art and Science University of Chiapas	N/A	2017 to 2018
Land surface temperature	Landsat 5 scenes	US Geological Service (https://earthexplorer.usgs.gov/)	30 m	April 5, 2001 April 1, 2011
	Landsat 8 scenes		30 m	April 1, 2017
Real color image of high resolution	Unknown	Ministry of Environment and Natural History in Chiapas (SEMAHN)	0.5 m	2015
Mosaic of Panchromatic Image of high resolution	Unknown	National Institute of Statistics, Geography and Informatics (INEGI)	1.5 m	2001
Surface temperature	Infrared thermometer Extech brand model IR201A	N/A	N/A	Field campaign May 29 and 30, 2019

Table II. Metadata of Landsat imagery.

Satellite	Sensor	Pixel size (m)	Nubosity (%)	Date	Hour center of the scene
LandSat 5	TM	30	5%	April 5, 2001	16: 15: 36.6920500Z
LandSat 5	TM	30	6%	April 1, 2011	16: 25: 30.5330810Z
LandSat 8	OLI_TIRS	30	0.40%	April 1, 2017	16: 35: 15.5568250Z

temperatures defined by The Territory and Urban Development Ministry (SEDATU, 2014) as reference values for the analysis of results (Table III).

Most LST research has been done during the dry season because cloud cover is low and higher atmospheric humidity can increase the error of emissivity and temperature. For this reason, we confined our research to the dry season in TGZ.

To calculate LST, we applied conventional and thermal remote sensing corrections to the three scenes downloaded (Chander *et al*., 2009; USGS, 2013)Top-Of-Atmosphere (TOA. This correction was done in two stages. First, we considered the build-up of an emissivity layer according to the ECM, then, we retrieved LST by transforming thermal brightness (Figure 4). The combination of band thermal and radiometric correction (Figure 4), allowed to obtain LST values for each image.

Though atmospheric conditions are the main source of error for LST retrieval (Cook *et al*., 2014),

Table III. Vegetation and human vulnerability due to extreme air temperatures.

Temperatures	Class	Vulnerability
< 28 °C	Pleasant	Comfortable wellness
28 a 31 °C	Discomfort	Evapotranspiration increases. Headaches increase in humans.
31.1 a 33 °C	Extreme discomfort	Dehydration is evident. Hoppers and heavy pollution particle pollution increases, appearing at cities.
33.1 a 35 °C	Stress condition	Plants evapotranspire excessively and wilt. Forest fire hazard increases.
> 35 °C	Upper tolerance limit	Heat strokes occur, with unconsciousness in some people. The diseases increase.

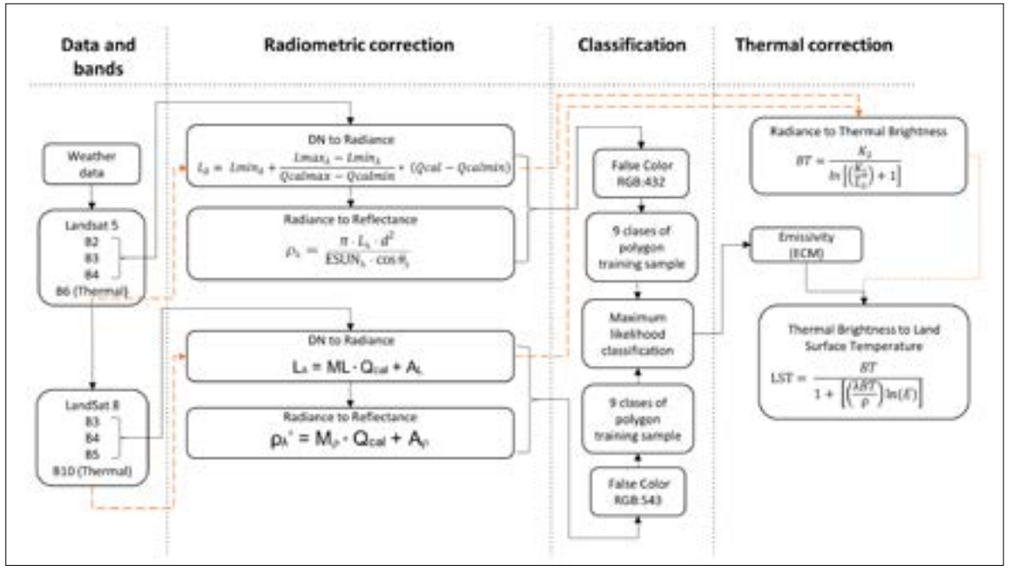

Figure. 2. Diagram for land surface temperature (LST) retrieve based on Landsat imagery. Dash arrows indicate the band thermal correction process up to the thermal brightness while the radiometric correction and supervised classification to assign emissivity is indicated by the black arrows.

we made no correction of this sort due to a lack of information on relative humidity, wind speed, and atmospheric pressure.

Land use-land cover image classification

We radiometrically corrected each band of the images up to reflectance (Table IV) using equations 1 and 2 (Chander *et al*., 2009)Top-Of-Atmosphere (TOA. The correction served to sort the images, into nine LULC classes and thereby assign an emissivity value to each class.

$$L_\lambda = Lmin_\lambda + \frac{Lmax_\lambda - Lmin_\lambda}{Qcalmax - Qcalmin} * (Qcal - Qcalmin) \quad (1)$$

$$\rho_\lambda = \frac{\pi \cdot L_\lambda \cdot d^2}{ESUN_\lambda \cdot \cos\theta_s} \quad (2)$$

Based on a high-resolution images and the orthophoto mosaic, we generated for each image classification training polygons consisting of nine classes of LULC (Table IV). These polygons were used to train a maximum likelihood algorithm (MAXLIKELIHOOD) and classify each image (Melesse *et al*., 2007; Sobrino *et al*., 2012).

The bare soil class denotes areas where the surface consists of bedrock (mainly limestone). The bare agriculture soil class denotes agriculture soil without vegetative cover. The rest of the classes are self-explanatory (Table V).

Emissivity Classification Method (ECM)

Emissivity Classification Method (ECM), which assigns emissivity values based on previous measurements or from libraries such as the ASTER Spectral Library (ASL, https://speclib.jpl.nasa.gov/) to generate land use and land cover (LULC) classification (Sobrino *et al.,* 2012)

We applied ECM for emissivity retrieval (Table V) to avoid homogenizing the entire urban area into two or three values of emissivity, which would have happened if we relied on $NDVI^{THM}$.

Land surface temperature (LST) retrieval

Once an emissivity raster coverage was estimated, LST values were obtained, following equation 1. We applied radiometric correction of thermal

Table IV. Radiometric correction parameters for TM 5 and OLI 8 sensors.

TM 5 Sensor, 2001 year							
Band	QcalMAX	QcalMIN	LMAX	LMIN	d	ESUN	SZ
2	255	1	365	-2.84		1796	
3	255	1	264	-1.17	1.0005897	1536	31.31
4	255	1	221	-1.51		1031	
2011 year							
2	255	1	365	-2.84		1796	
3	255	1	264	-1.17	0.999269	1536	30.13
4	255	1	221	-1.51		1031	
OLI 8 Sensor, 2017 year							
	ML	AL	Mp	Ap	d		SZ
3	0.011861	-59.3059					
4	0.010002	-50.0101	0.00002	-0.1	0.9994378		27.84
5	0.0061207	-30.6037					

* Qcalmin = Minimum quantized value of pixel [dimensionless], Qcalmax = Maximum quantized value of pixel [dimensionless], LMIN = Spectral at-sensor radiance that is scaled to Qcalmin [W/(m2 sr μm)], LMAX = Spectral at-sensor radiance that is scaled to Qcalmax [W/(sr m2 sr μm)], ESUN= Mean exoatmospheric solar irradiance [W/(m2 μ m)], Angle SZ= Solar zenith angle [degrees] (Chander et al., 2009; USGS, 2013).

Table V. Emissivity values by type of sensor (TM 5 and OLI 8) and LULC classes.

Sensor	TM 5	OLI 8
Band	B6	B10
Range (μm)	10.4 a 12.5	10.6 a 11.19
Water*	0.99	0.99
Trees+	0.99	0.99
Asphalt road+	0.963	0.962
Green grass*	0.981	0.98
Bare soil+	0.956	0.942
Bare agriculture soil*	0.968	0.941
Concrete ceiling+	0.957	0.943
Metal ceiling*	0.046	0.049
Roof tile ceiling+	0.942	0.939

* Source: Aster Spectral Library. +Source: (Sobrino *et al.*, 2012)

* Source: Aster Spectral Library. +Source: (Sobrino *et al.*, 2012)

bands up to radiance. Then, using equation 3 (Chander *et al.*, 2009)Top-Of-Atmosphere (TOA and conversion from Kelvin to Celsius degrees with equation 4, we estimated thermal brightness values from radiance.

$$TB = \frac{K_2}{ln\left[\left(\frac{K_1}{L_\lambda}\right)+1\right]} \quad (3)$$

$$TB_C = TB - 273.15 \quad (4)$$

Finally, we calculated per-pixel LST using equation (5):

$$LST = \frac{TB_c}{1+\left[\left(\frac{\lambda TB_c}{\rho}\right)\ln(E)\right]} \quad (5)$$

TB is the thermal brightness [K]; TB_c is the thermal brightness in Celsius degrees [C]; LST is the land surface temperature in Celsius degrees [C]; K_1 is the first calibration constant [W/ (m^2 sr μm)]; K_2 second calibration constant [K]; L_λ is the spectral radiance at-sensor [W/(m^2 sr μm)]; ln is natural logarithm; E is the emissivity; λ is the center of the thermal band [μm]; ρ is a constant that combines the Boltzman and Plank´s Law and the speed of light with a value of 14,387.7 [μmºC] (Table VI).

RESULTS AND DISCUSSION

Daily air temperature data, from 1951 to 2016, showed that after 1980 temperatures above 40 °C have become more frequent by a rate of 18% and minimum air daily temperatures above 28 °C have increased by a rate of 14%.

Hourly records from 2013 to 2018 show that maximum daily temperatures occur between 14:10 and 17:00 hrs. Daytime temperatures, between 06:00 and 19:59 hrs, range from 8.6 °C to 48.4 ºC. Nighttime temperatures, between 20:00 and 05:59 hrs, range from 9.2 °C to 32.5 °C. During the time scale study, 60% of daytime temperatures and 63% of nighttime temperatures occurred between 25 °C to 30 °C, suggesting that nights are as warmer as days in TGZ (Figure 3), but it is necessary to continue registering hourly air temperatures to confirm this trend.

As there are no weather stations located on the periphery of the city, we were unable to compare temperatures in the city center and the surrounding rural areas. In addition, there are no night Landsat images that record land surface temperature that would allow us to study diurnal variation in UHI.

On average, the hottest months, are April and May, with average daily temperature of 27.2 and 27.8 °C, respectively. During these months, the maximum temperatures occur with clear skies and low relative humidity, ideal conditions for classification of LULC and LST retrieval (Figure 4).

This information was used to determine the Landsat scenes (Table II) in order to reach an optimum accuracy of the classification processes (Table VII).

The classification processed showed that tree coverage decreased by 21% in TGZ (Table VIII).

Table VI. Thermal correction parameters to estimate the thermal brightness values.

Sensor TM 5		
Band	K1	K2
6	607.76	1260.56
Sensor TIRS 8		
10	774.89	1321.08

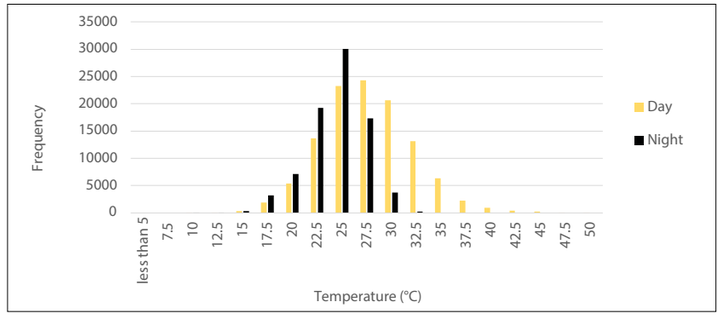

Figure 3. Thermal hourly distribution registered at day and night in the city of Tuxtla Gutiérrez from years 2013 to 2018.

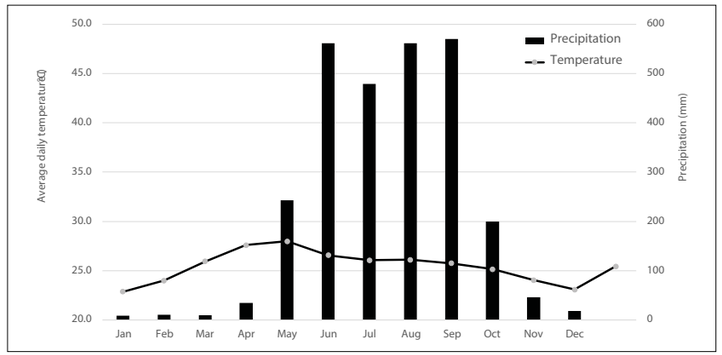

Figure 4. Average daily temperature and precipitation for the city of Tuxtla Gutiérrez, from 1951 to 2016 year.

Table VII. Landsat images classification accuracy.

Sensor	Year	Overall accuracy (%)
TM 5	2001	80.86
TM 5	2011	86.33
OLI 8	2017	85.44

Table VIII. Land use/land cover percentage across the city of Tuxtla Gutiérrez, Chiapas in 2001, 2011 and 2017.

Class	Land coverage	2001 (%)	2011 (%)	2017 (%)
1	Water	0.02	0.01	0.02
2	Trees	17.63	14.25	13.98
3	Asphalt road	9.3	13.22	12.95
4	Green grass	1.8	2.14	1.65
5	Bare soil	2.67	4.53	7.75
6	Bare agriculture soil	34.77	20.32	11.34
7	Concrete ceiling	18.29	28.98	35.54
8	Metal ceiling	1.4	2.85	2.6
9	Roof tile ceiling	14.12	13.71	14.16

This loss of tree cover was concentrated along the Sabinal River, Botanical Garden, Zoo, some urban parks, and natural reserves areas on the south of the city (Figures 6 to 8).

The LST distribution for the three years of the study are given in Table IX and Figure 5.

There are street trees in the area but quantifying their impact on temperature and surface

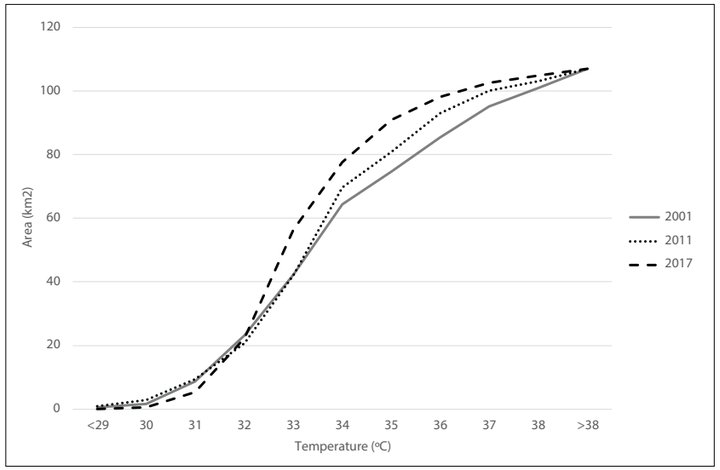

Figure 5. Total area for each land surface temperature (LST) range analyzed in the years of study.

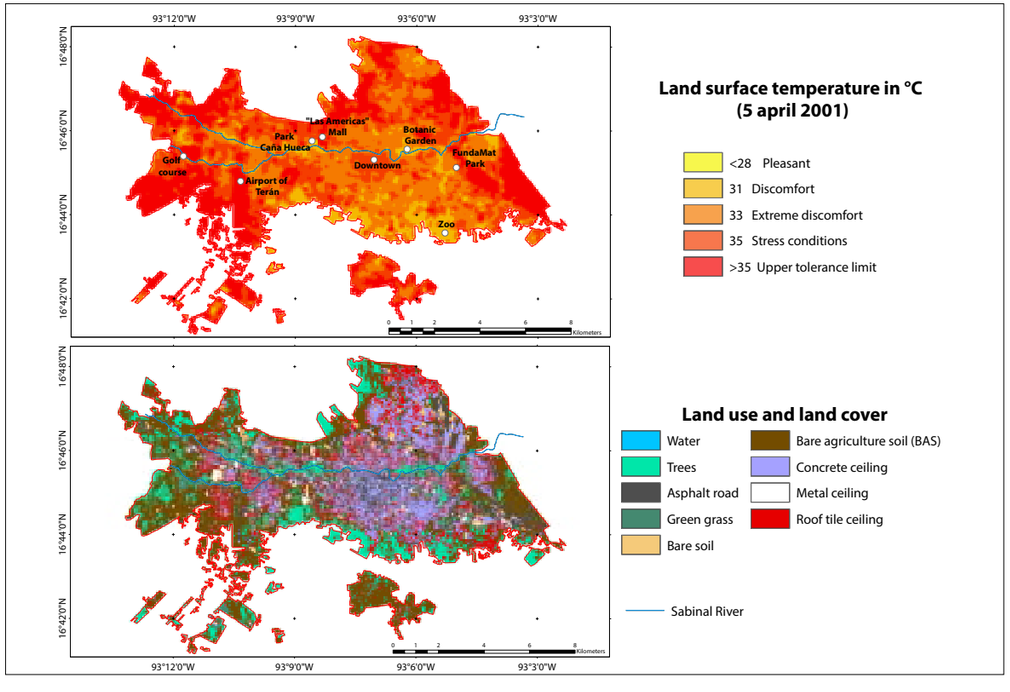

Figure 6. Land surface temperature and land cover during April 5th, 2001 in the city of Tuxtla Gutiérrez, Chiapas.

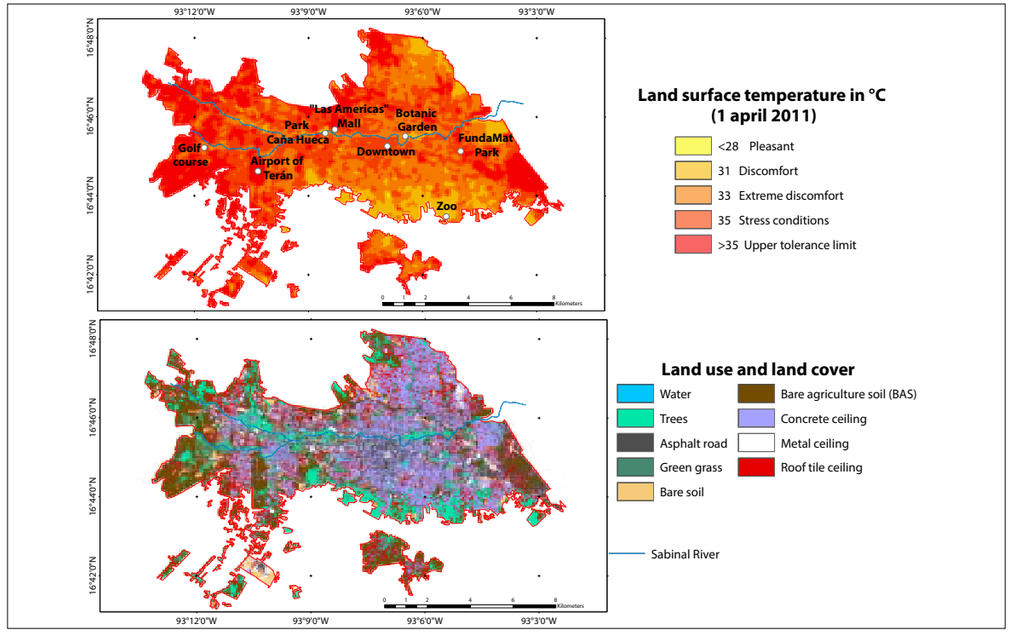

Figure 7. Land surface temperature and land cover during April 1st, 2011 in the city of Tuxtla Gutiérrez, Chiapas.

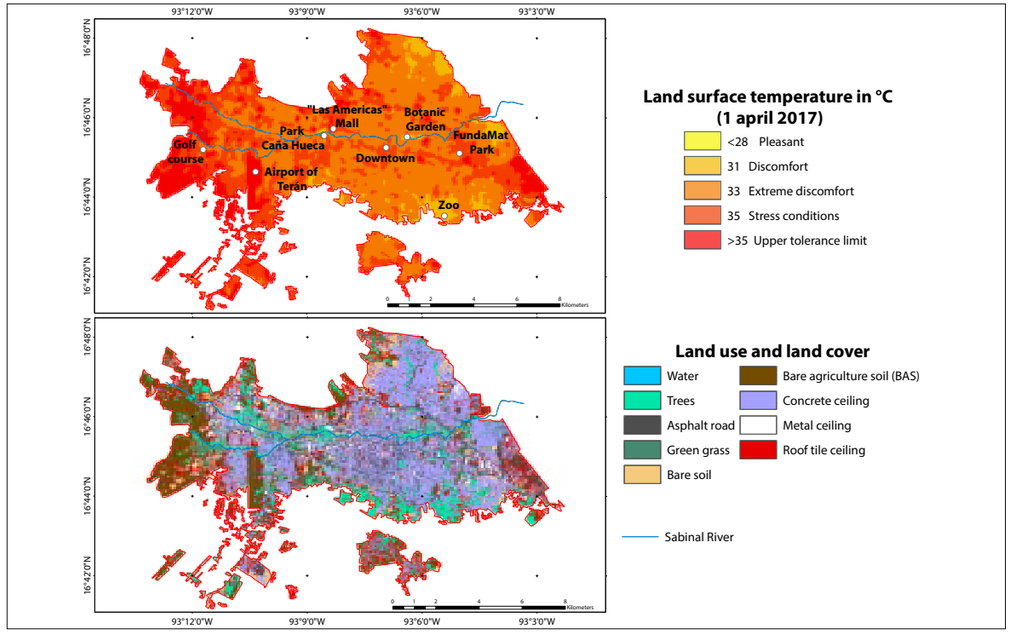

Figure 8. Land surface temperature and land cover during April 1st, 2017 in the city of Tuxtla Gutiérrez, Chiapas.

Table IX. Tuxtla Gutierrez (TGZ) surface percentage per vulnerability class based on land surface temperature (LST) for the years 2001, 2011 and 2017.

	2001	20011	2017
	(%)	(%)	(%)
Pleasant (<29 °C)	0.5	0.8	0.04
Discomfort (29 to 31 °C)	7.6	8	4.96
Extreme discomfort (31 to 33 °C)	31.4	30.5	47.8
Stress condition (33 to 35 °C)	30.1	36.2	32.1
Upper tolerance limit (>35 °C)	30.4	24.5	15.1

variation requires finer-resolution imagery, species identification and tree health recognition (Román, 2017). In the southwestern part of the city, where substantial residential development took place during the early 2000s (Silva *et al*., 2015), vegetation coverage has decreased and BAS, concrete, and roof tile ceiling has increased. This change in land cover was accompanied by temperature changes in TGZ. Specifically, temperatures shifted from discomfort temperatures (29 °C to 31 °C) in 2001 to extreme discomfort (31 °C to 33 °C) and stress condition temperatures (33 °C to 35 °C) in 2011 and 2017, respectively.

The urban tree land-cover class had the lowest LST. In 2001, around 25% of urban tree areas were located at pleasant to discomfort temperatures zones, reaching only 11% by 2017. Large continuous areas of dense tree cover had the lowest LST, for example, parks such as Caña Hueca, Joyyo Mayu, Tuchtlán, Botanical Garden, Parque Oriente and Parque Patricia, with areas from 3 to 20 ha, registered temperatures below 28 ºC LST. By contrast, parks smaller than 3 ha or with very dispersed and low tree density, such as urban parks or wasteland (1.3 to 13.3 ha), had higher temperatures (Figure 9). It is evident at the spatial scale of the present study, that the Sabinal River has a cooling effect (Figure 6 to 8), which crosses the city in the west-east direction, and its riparian vegetation. For the three years analyzed, we observed that along this main-channel, and in its open sky sections the maximum temperatures ranged from 28 to 35 ºC. We observed, the same mitigating effect in other tributary channels to the east of the city.

Figure 9. Comparison of land surface temperature (LST) registered at two contiguous woodland areas with different tree density.

The BAS class is made up of dark soil clays (mainly Vertisols, Regosols, and Leptosols) devoid of vegetation that is distributed at the periphery of the city. Its extent decreased 67% (3,650 to 1,214 ha) between 2001 and 2017, changing into roof tile ceiling, asphalt road, and concrete ceiling classes. For the three years analyzed, BAS mean temperature was 35 °C, but when it changes into asphalt road its mean value decreased 1 °C for and 3 °C for concrete ceiling. Thermal characteristics of soil and the day/night behavior of UHI highly influence the BAS class.

Soil physicochemical characteristics determine its capacity to absorb and retain heat. Dark and damp soils with high organic matter content tend to retain a greater amount of caloric energy and lose it more slowly. By contrast, light, stony and dry soils have a heterogeneous behavior; they can be heated considerably but also lose energy quickly or absorb it at lower rates and therefore show less caloric emission (Owens and Rutledge, 2005). Climate also influences soil temperature; in tropical regions soils tend to have higher temperatures (from 2 to 4 °C above the AT), due to microbial activity, compared to soils of the same type in temperate regions (Buol, 2005).

Vertisols are dark soils, with a high content of clays considered isohyperthermic, thermal and mesic (Virmani *et al*., 1982; Palma-lópez *et al*., 2002; FAO, 2007). These are the type of BAS that presents the maximum retrieve LST for the three dates of the present study. They are located on the west of the city, as temporary agricultural land at rest; that is, without crops at the time the images were acquired. During field verification we observed moisture and stubble. This land use faces conversion pressure, as 11 residential developments were registered nearby.

Leptosols and Regosols are shallow, stony, grouped as Entisols, and are considered hyperthermic and thermal soils (Lorenz, 1995; Palma-López *et al*., 2002; FAO, 2007). Leptosols are located on the north and east of the city on steep slopes. Between 2000 and 2015 these areas showed the greatest urban sprawl and land conversion. Now, however, they are areas of conservation. On the other hand, Regosols are located on the south of the city. Their thermal behavior is the most heterogeneous. They register temperatures lower than 28 °C to 39 °C. Possibly due to the stony conditions, Regosols´ temperature rises considerably during the day, but drops quickly in cloudy conditions, or at night. However, this behavior has not been verified since there are no Landsat scenes of the study area at night.

The physical characteristics of each land coverage are also related to the day/night behavior of UHI, a phenomenon that has been extensively discussed (Oke *et al*., 1991; Jauregui, 1997; Prakash *et al.,* 1999; Azevedo *et al*., 2016; Ando and Ueyama, 2017; Kato *et al*., 2018). Bohnenstengel *et al*. (2011), simulated the behavior of the UHI in the city of London, evaluating the energy flow hourly. The study found that the temperatures of rural and urban areas depend on thermal inertia. Usually, thermal inertia of rural areas is low. Increasing LST in rural areas, requires less energy than doing so urban areas. Nevertheless, diurnal behavior of both areas, rural and urban, depends not only on thermal inertia but also on cloudiness, relative humidity, direction and speed of wind, and constructive materials. Similar observations in Arizona and Mexico City where peri urban areas recorded higher temperatures than cities´ downtowns during the day and the inverse behavior at nights (Jauregui, 1997; Tejeda-Martínez and Jáuregui-Ostos, 2005; Imhoff *et al*., 2010; Ruddell and Dixon, 2014).

Areas with both, metal ceiling and asphalt roads, such as malls like Plaza de las Americas, Plaza Cristal and Plaza Polyforum showed thermal peaks (temperature above 40 °C). These results described are consistent with those reported by Coello (2015) who used a thermographic camera to retrieve temperatures for different coverages at the main campus of The University of Science and Art of Chiapas between 13:00 and 15:00 hrs. Coello reported that maximum temperatures occurred at the metal ceiling of sport courts (60.5 °C), followed by football camp with synthetic grass (55 to 59 °C), bare soil with the large range of temperature variation (46 to 58 °C), asphalt roads (52 to 57 °C), concrete (47 to 54 °C), scattered vegetation (33 to 38 °C) and swimming pool (28 to 29 °C) (Coello, 2015).

One transect profile was generated across TGZ form east to west direction to validate the changes in LST due to of land cover changes occurring from 2001 to 2017 (Figure 10). LST has increased due to transformation of trees into SDA or non-evaporating surfaces and decreased when land converted to trees (Table X).

The mean temperatures reported at Table X were those occurring at transect profile (Figure 10). The highest increase in LST occurred when trees became BAS (3 °C), followed by asphalt road (1.7 °C) and bare soil/concrete ceiling (1.4-1.3 °C). On the other hand, TGZ city had reforestation programs at median strips, parks and vacant lots in 2005 and 2016, and these programs appear to have a modest cooling effect flourishing (0.1 and 1.2 °C) by 2017 year.

On the 29th and 30th of May 2019 (Table XI) between 15:00:00 and 17:17:00 hrs, temperature verification performed in 10 sites across the city of

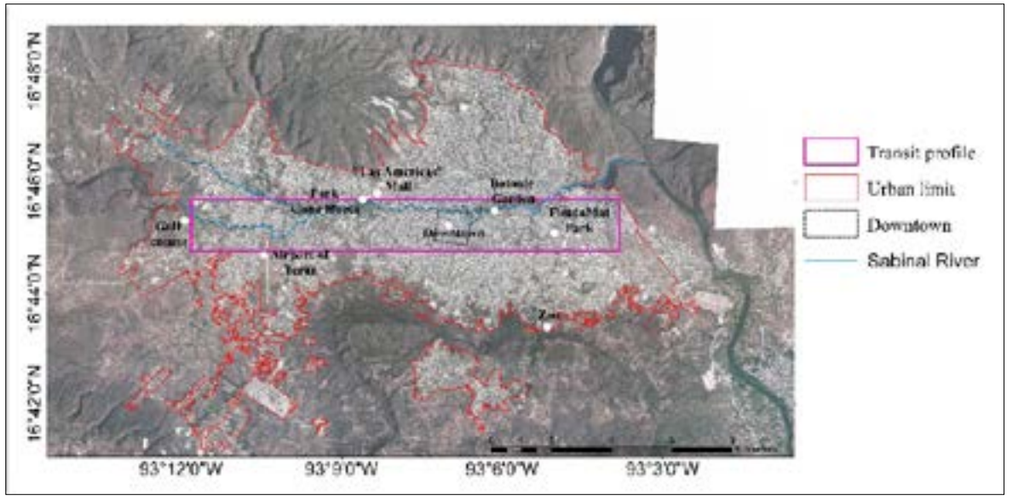

Figure 10. Transect profile across the city of Tuxtla Gutiérrez, Chiapas used for validating the relation of land surface temperature (LST) with land use and land change cover.

Table X. Land surface temperature (LST) variation in response to land use/land cover changes.

Land use/land cover change	Area (ha)	Mean Temp. (°C) 2001	Mean Temp. (°C) 2017	Average change in LST (°C) 2001-2017
Tree to asphalt road	30.33	32.27	33.99	1.7
Tree to bare soil	21.69	32.27	33.64	1.4
Tree to BAS	13.23	32.27	35.34	3.1
Tree to concrete ceiling	64.7	32.27	33.6	1.3
Asphalt to tree	6.8	33.1	32.9	-0.1
BAS* to tree	20.5	35.0	33.8	-1.2

* BAS = bare agriculture soil.

Table XI. Land surface temperatures at verification sites.

Site	Colony	Description	Latitude	Longitude	Temperature (°C) 29 May	Temperature (°C) 30 May	Notes
UNICACH, University City	Canteras	Football field	16.78	-93.12	45.0	34.0	Synthetic open pit grass
SEMAHN	Rivera Cerro Hueco	Parking lot	16.73	-93.09	43.7	32.3	Asphalt and stone
Market Dr. Rafael Pascacio Gamboa	El Calvario	Market with metal ceiling	16.75	-93.12	45.0	34.7	Area with high vehicular traffic and little vegetation cover
Plaza Del Sol (De las Américas)	Joyo Mayyu	Parking lot	16.76	-93.14	40.8	35.3	Asphalt
Terán airport	Militar base air	Hill with bare soil vertisol	16.74	-93.18	43.8	34.1	Constant burning for weed management, vertisol, black soil
Site 01	Nameless	Burned agricultural field	16.77	-93.20	42.5	33.8	Bare regosol, brown soil
Site 02	Nameless	Agricultural field without stubble	16.74	-93.22	49.6	40.3	Bare vertisol, black soil
Site 03	Satélite (Loma Larga)	Base soil	16.74	-93.05	50.7	48.0	Bare leptosol, black soil, stony
UNICACH, Plastic Arts Campus	Tzocotumbak	Football field	16.75	-93.10	41.0	37.1	Synthetic open pit grass
Road	Road to Vicente Guerrero	Asphalt	16.74	-93.21	46.8	36.8	Asphalt road near vertisol soil fields

TGZ. The sites were chosen considering the areas that reported high LST during 2017. May 29th presented sunny conditions, while May 30th was cloudy with drizzle. On both dates, the maximum temperatures were recorded on site 03, in the east of the city, which had BAS Leptosol with pebbly black earth. The second highest temperatures appeared on site 02, in the west, with BAS Vertisol and black soil with residual stubble. Synthetic pit grass was the second warmest coverage, followed by asphalt. Direct temperature measurement showed the same relative patterns, although there were some differences between directly measured and remotely sensed temperatures.

Notwithstanding, this study was limited by the resolution and only day time availability of the satellite imagery, the previous studies (Coello, 2015) and verification performed supported the trend of the different land uses and coverages in relation with LST. The direction of land use change determines the raised or decreased of LST, but in general, when vegetation is transformed into any

other land use the LST increased at least 1 °C and decreased the same in the opposite direction. The minimum variation of LST detected in land use change from asphalt to tree (-0.1 °C) may be caused by the imagery resolution (30 m per pixel) and height of trees, since reforestation programs are recent, and according to Coello (2015), the refreshing effect of vegetation may be more than 10 °C in comparison with asphalt and BAS cover.

The cooling effect of vegetation in tropical cities may contribute to the wellbeing of the population by mitigating UHI, but more studies are needed in economic and social terms in each city for a strategy to determine the sites and area of reforestation, the maintenance work required, the best species for reforestation and the availability of soil and water needed.

CONCLUSIONS

For the city of TGZ, the materials with the highest thermal sensitivity were BAS and asphalt roads. The change of tree cover into asphalt road, bare soil or BAS cover caused LST increased 1 °C to 3 °C. When asphalt or BAS cover classes turned into the tree class, LST decreased from 0.1 °C to 1 °C, suggesting that the cooling effect of trees is not immediately reached after reforestation. The vegetation effect in LST is appraised if woodlands are greater than 3 ha indicating a limitation of the analysis caused by the spatial resolution of the imagery used.

The ECM for the thermal assessment captured the surface heterogenicity of the TGZ city avoiding underestimations induced for NDVI methodologies. Nevertheless, the *in-situ* measures of emissivity values and night temperature assessment will improve results and are desirable for further investigations.

The approach implemented in this study to carry out the analysis could be used to evaluate the surface thermal dynamic of cities when monitoring weather networks are not available or are not wide enough to cover the study area properly.

REFERENCES

Ali, J. M., Marsh, S. H., and Smith, M. J. (2016). Modelling the spatiotemporal change of canopy urban heat islands. *Building and Environment*, *107*, 64–78. https://doi.org/10.1016/j.buildenv.2016.07.010

Amanollahi, J., Tzanis, C., Firuz, M., and Makmom, A. (2016). Urban heat evolution in a tropical area utilizing Landsat imagery. *Atmospheric Research*, *167*, 175–182. https://doi.org/10.1016/j.atmosres.2015.07.019

Ando, T., and Ueyama, M. (2017). Surface energy exchange in a dense urban built-up area based on two-year eddy covariance measurements in Sakai, Japan. *Urban Climate*, *19*, 155–169. https://doi.org/10.1016/j.uclim.2017.01.005

Avdan, U., and Jovanovska, G. (2016). Algorithm for Automated Mapping of Land Surface Temperature Using LANDSAT 8 Satellite Data. *Journal of Sensors*, *2016*, 1–8.

Azevedo, J. A., Chapman, L., and Muller, C. L. (2016). Quantifying the daytime and night-time urban heat Island in Birmingham, UK: A comparison of satellite derived land surface temperature and high resolution air temperature observations. *Remote Sensing*, *8*(153), 1–17. https://doi.org/10.3390/rs8020153

Britter, R. E., and Hanna, S. R. (2003). Flow and Dispersion in Urban Areas. *Annual Review of Fluid Mechanics*, *35*, 469–496. https://doi.org/10.1146/annurev.fluid.35.101101.161147

Buol, S. (2005). Tropical soils. Soil-temperature regimes of Tropics. In *Encyclopedia of Soils in the Environment* (pp. 187–200).

CEIEG. (2014). *Municipio tuxtla gutiérrez*. Recuperado de: http://www.ceieg.chiapas.gob.mx/perfiles/Inicio

Chander, G., Markham, B., and Helder, D. (2009). Summary of current radiometric calibration coefficients for Landsat MSS, TM, ETM +, and EO-1 ALI sensors. *Remote Sensing of Environment*, *113*(5), 893–903. https://doi.org/10.1016/j.rse.2009.01.007

Chen, F., Yang, S., Yin, K., and Chan, P. (2017). Challenges to quantitative applications of Landsat observations for the urban thermal environment. *Journal of Environmental Sciences*, *59*, 80–88. https://doi.org/10.1016/j.jes.2017.02.009

Coello, M. E. (2015). Impacto de la Isla de Calor Urbana en el consumo energético por refrigeración de edificios en Ciudad Universitaria, UNICACH. Universidad de Ciencias y Artes de Chiapas.

Cogliati, M. (2011). Temperatura de superficie en el Valle del Río Neuquén utilizando imágenes Landsat. *Boletín Geográfico*, *33*, 11–26. Recuperado de: https://dialnet.unirioja.es/servlet/articulo?codigo=5017815

Cook, M., Schott, J. R., Mandel, J., and Raqueno, N. (2014). Development of an operational calibration methodology for the Landsat thermal data archive and initial testing of the atmospheric compensation component of a land surface temperature (LST) product from the archive. *Remote Sensing*, *6*, 11244–11266. https://doi.org/10.3390/rs61111244

De la Mora, C., Ruíz, J., Flores, H., Zarazúa, P., Ramírez, O., Medina, G., Rodríguez, V., and Chávez, Á. (2016). Índices de cambio climático en el estado de Chiapas 1960 -2009. *Revista Mexicana de Ciencias Agrícolas*, *13*, 2523–2534. Recuperado de: http://www.scielo.org.mx/pdf/remexca/v7nspe13/2007-0934-remexca-7-spe13-2523.pdf

Díaz-Nigenda, E., Tatarko, J., Morales-Iglesias, H., Méndez-Hernández, Z., Morales-Vázquez, W., and Alatorre-Ibargüengoitia, M. A. (2018). Measurement and modeling air quality impacts of dust emissions from unpaved roads in Tuxtla Gutierrez, Chiapas. *Geosciences*, *8*(284), 16. https://doi.org/10.3390/geosciences8080284

Eniolu, T., Adedoyin, A., and Bayode, O. (2013). Urban Climate Comparing the effect of trees on thermal conditions of two typical urban buildings. *Urban Climate*, *3*, 76–93. https://doi.org/10.1016/j.uclim.2013.04.002

Ermida, S. L., DaCamara, C. C., Trigo, I. F., Pires, A. C., Ghent, D., and Remedios, J. (2017). Modelling directional effects on remotely sensed land surface temperature. *Remote Sensing of Environment*, *190*, 56–69. https://doi.org/10.1016/j.rse.2016.12.008

FAO. (2007). Base Referencial Mundial del Recurso Suelo. Primera actualización 2007. In *Informes sobre Recursos Mundiales de Suelos No. 103*. Recuperado de: http://www.fao.org/3/a0510s/a0510s00.pdf

García-Cueto, O. R., Tejeda-Martínez, A., and Bojórquez-Morales, G. (2009). Urbanization effects upon the air temperature in Mexicali, B. C., México. *Atmosfera*, *22*(4), 349–365. Recuperado de: http://www.scielo.org.mx/scielo.php?script=sci_arttext&pid=S0187-62362009000400002

Gulbe, L., Caune, V., and Korats, G. (2017). Urban area thermal monitoring: Liepaja case study using satellite and aerial thermal data. *International Journal of Applied Earth Observation and Geoinformation*, *63*, 45–54. https://doi.org/10.1016/j.jag.2017.07.005

HATG. (2007). Programa de Desarrollo Urbano del Centro de Población de Tuxtla Gutiérrez, Chiapas. Recuperado de: https://tuxtla.gob.mx/pg/muni/archivos/transparencia-fiscal/1-marco-regulatorio/6-1-programa-de-desarrollo-urbano-de-tuxtla-2007.pdf

Howard, L. (1988). The Climate of London. In *International Association for Urban Climate*. International Association for Urban Climate. https://doi.org/10.1177/0309133309339794

ICIPLAM. (2013). Agenda Estratégica de Nuestra Ciudad, Tuxtla 2030. Instituto Ciudadano de Planeacion Municipal de Tuxtla. Recuperado de: http://www.tuxtla.gob.mx/iciplam/descargas/Tuxtla2030.pdf

ICIPLAM. (2015). Valoración de los parques urbanos. La ruta hacia una Tuxtla sustentable. Instituto Ciudadano de Planeacion Municipal de Tuxtla. Recuperado de: https://tuxtla.gob.mx/iciplam/descargas/VALORACION-DE-LOS-PARQUES-URBANOS-2015.pdf

Imhoff, M. L., Zhang, P., Wolfe, R. E., and Bounoua, L. (2010). Remote sensing of the urban heat island effect across biomes in the continental USA. *Remote Sensing of Environment*, *114*, 504–513. https://doi.org/10.1016/j.rse.2009.10.008

INEGI. (2013). *Datos Generales de Microrregiones: Tuxtla Gutiérrez*. Recuperado de: http://www.microrregiones.gob.mx/zap/datGenerales.aspx?entra=nacion&ent=07&mun=101

INEGI. (2017). Anuario estadístico y geográfico de Chiapas 2017 (317.2; Anuarios Estadísticos). Recuperado de: https://www.datatur.sectur.gob.mx/ITxEF_Docs/CHIS_ANUARIO_PDF.pdf

IPCC. (2018). Resumen para responsables del políticas. In V. Masson-Delmotte, H.-O. Pörtner, P. Zhau, D. Roberts, J. Skea, P. Shukla, A. Pirani, W. Moufouma-Okia, C. Péan, R. Pidcock, Y. Chen, S. Connors, X. Zhoum, R. Mattews, M. Gomis, E. Lonnoy, T. Maycock, M. Tignor, & T. Waterfield (Eds.), *Calentamiento global de 1,5 °C, Informe especial del IPCC sobre los impactos del calentamiento global de 1,5 °C con respecto a los niveles preindustriales y las trayectorias correspondientes que deberían seguir las emisiones mundiales de gases de efecto i*. The Intergovernmental Panel of Climate Change. Recuperado de: https://www.ipcc.ch/site/assets/uploads/sites/2/2019/09/IPCC-Special-Report-1.5-SPM_es.pdf

Jauregui, E. (1997). Heat Island Development In Mexico City. *Atmospheric Environment*, *31*(22), 3821–3831. https://doi.org/10.1016/S1352-2310(97)00136-2

Jeevalakshmi, D., Narayana, S., and Manikiam, B. (2017). Land Surface Temperature Retrieval from LANDSAT data using Emissivity Estimation. *International Journal of Applied Engineering Research*, *12*(20), 9679–9687. Recuperado de: https://www.ripublication.com/ijaer17/ijaerv12n20_57.pdf

Kahle, A. (1987). Surface emittance, temperature, and thermal inertia derived from Thermal Ifrared Multiespectral Scanner (TIMS) data for Death Valley, California. *Geophysics*, *52*(7), 858–874.

Kato, S., Kouyama, T., Nakamura, R., Matsunaga, T., and Fukuhara, T. (2018). Simultaneous retrieval of

temperature and area according to sub-pixel hotspots from nighttime Landsat 8 OLI data. *Remote Sensing of Environment*, *204*, 276–286. https://doi.org/10.1016/j.rse.2017.10.025

Li, H., Zhou, Y., Li, X., Meng, L., Wang, X., Wu, S., and Sodoudi, S. (2018). A new method to quantify surface urban heat island intensity. *Science of the Total Environment*, *624*, 262–272. https://doi.org/10.1016/j.scitotenv.2017.11.360

López-Pérez, L. A., Flores-Prieto, J. J., and Ríos-Rojas, C. (2019). Adaptive thermal comfort model for educational buildings in a hot-humid climate. *Building and Environment*, *150*(December 2018), 181–194. https://doi.org/10.1016/j.buildenv.2018.12.011

Lorenz, G. (1995). Caracterización ecológica de un suelo Eutric Regosol bajo bosque en el Chaco semiárico, Argentina. *Quebracho*, *3*, 13–23.

Mas, J.-F. (2011). Aplicación del sensor MODIS para el monitoreo del territorio. INE-SEMARNAT-UNAM-CIGA. Recuperado de: https://www.ciga.unam.mx/publicaciones/index.php/component/abook/book/12-coleccionesciga/1-aplicaciones-del-sensor-modis-para-el-monitoreo-del-territorio

Melesse, A., Weng, Q., Prasad, S., and Senay, G. (2007). Remote Sensing Sensors and applications in environmental resources mapping and modelling. *Sensors*, *7*, 3209–3241. https://doi.org/10.3390/s7123209

Oke, T. R. (1973). City size and the urban heat island. *Atmospheric Environment Pergamon Pres*, *7*, 769–779. https://doi.org/10.1016/0004-6981(73)90140-6

Oke, T. R. (1982). The energetic basis of the urban heat island. *Quarterly Journal of the Royal Meteorological Society*, *455*, 1–24. Recuperado de: http://www.patarnott.com/pdf/Oake1982_UHI.pdf

Oke, T. R., Johnson, G., Steyn, D., and Watson, I. (1991). Simulation of surface urban heat islands undel ideal conditions at night. Part 2:Diagnosis of causation. *Boundary-Layer Meteorology*, *53*, 339–358. https://doi.org/10.1524/slaw.1958.3.15.357

Olioso, A. (1995). Estimating the difference between brightness and surface temperatures for a vegetal canopy. *Agricultural and Forest Meteorology*, *75*, 237–242. https://doi.org/10.1016/0168-1923(94)02163-E

Owens, P. R., and Rutledge, E. M. (2005). Morphology, Soil Color. In *Encyclopedia of Soils in the Environment*.

Palma-lópez, D. J., García, S. S., Olán, J. J. O., Narcía, A. T., Espinoza, C. L., Cruz, J. Z., Ruiz, A., and Martel, M. A. C. (2002). Sistema integrado para recomendar dosis de fertilización en caña de azúcar (SIRDF). *Terra*, *20*, 347–358.

Prakash, A., Pereira, R., and Vekerdy, Z. (1999). Monitoring coal fires using multi-temporal night-time thermal images in a coalfield in north-west china. *International Journal of Remote Sensing*, *20*(14), 2883–2888. https://doi.org/10.1080/014311699211868

Rajagopalan, P., Lim, K. C., and Jamei, E. (2014). Urban heat island and wind flow characteristics of a tropical city. *Solar Energy*, *107*(107), 159–170. https://doi.org/10.1016/j.solener.2014.05.042

Reyes, M. E., and López, Á. F. (2011). Ciudades rurales en Chiapas: formas territoriales emergentes. *Argumentos*, *66*, 121–152. Recuperado de: http://www.scielo.org.mx/scielo.php?script=sci_arttext&pid=S0187-57952011000200006&lng=es&tlng=es

Romaguera, M., Vaughan, R. G., Ettema, J., Izquierdo-Verdiguier, E., Hecker, C. A., and van der Meer, F. D. (2018). Detecting geothermal anomalies and evaluating LST geothermal component by combining thermal remote sensing time series and land surface model data. *Remote Sensing of Environment*, *204*, 534–552. https://doi.org/10.1016/j.rse.2017.10.003

Román, L. M. (2017). Análisis del arbolado de alineación y la percepción de los habitantes en la ciudad de Tuxtla Gutiérrez, Chiapas. Recuperado de: https://repositorio.unicach.mx/handle/20.500.12114/1418

Rozenstein, O., Qin, Z., Derimian, Y., and Karnieli, A. (2014). Derivation of land surface temperature for landsat-8 TIRS using a split window algorithm. *Sensors*, *14*, 5768–5780. https://doi.org/10.3390/s140405768

Ruddell, D. M., and Dixon, P. G. (2014). The energy-water nexus: are there tradeoffs between residential energy and water consumption in arid cities? *International Journal of Biometeorology*, *58*(7), 1421–1431. https://doi.org/10.1007/s00484-013-0743-y

SEDATU. (2014). Bases para la Estandarización en la Elaboración de Atlas de Riesgos y Catálogo de Datos Geográficos para Representar el Riesgo 2013. Recuperado de: https://www.gob.mx/cms/uploads/attachment/file/40838/Bases_AR_PRAH_2014.pdf

Silva, M., García, A., and Hernando, A. (2015). Crecimiento de la mancha urbana en la Zona Metropolitana de Tuxtla Gutiérrez (Chiapas , México). *Quehacer Científico En Chiapas*, *10*(2), 35–41. Recuperado de: http://www.dgip.unach.mx/index.php/directorio/revista-quehacer-cientifico

Sobrino, J., Jiménez-muñoz, J. C., Sòria, G., Romaguera, M., Guanter, L., Moreno, J., Plaza, A., Martínez, P., Member, A., Plaza, A., Member, S., and Martínez, P. (2008). Land surface emissivity retrieval from different VNIR and TIR sensors. *IEEE Transactions on Geoscience and Remote Sensing*, *46*(2), 316–327. https://doi.org/10.1109/TGRS.2007.904834

Sobrino, J., Jiménez-Muñoz, J., and Paolini, L. (2004). Land surface temperature retrieval from LANDSAT TM 5. *Remote Sensing of Environment*, *90*, 434–440. https://doi.org/10.1016/j.rse.2004.02.003

Sobrino, J., Oltra-Carrió, R., Jiménez-Muñoz, J. C., Julien, Y., Sòria, G., Franch, B., and Mattar, C. (2012). Emissivity mapping over urban areas using a classification-based approach: Application to the Dual-use European Security IR Experiment (DESIREX). *International Journal of Applied Earth Observation and Geoinformation*, *18*, 141–147. https://doi.org/10.1016/j.jag.2012.01.022

Suomi, J. (2014). Characteristics of Urban Heat Island (UHI) in a high-latitude coastal city-a case of study of Turku, SW Finland [University of Turku]. Recuperado de: https://www.utupub.fi/bitstream/handle/10024/101035/AnnalesAII295.pdf?sequence=2&isAllowed=y

Tan, K., Liao, Z., Du, P., and Wu, L. (2017). Land surface temperature retrieval from Landsat 8 data and validation with geosensor network. *Frontiers of Earth Science*, *11*(1), 20–34. https://doi.org/10.1007/s11707-016-0570-7

Tejeda-Martínez, A., and Jáuregui-Ostos, E. (2005). Surface energy balance measurements in the México City region: A review. *Atmosfera*, *18*(1), 1–23.

UN. (2018). The World's Cities in 2018. In *United Nations, Department of Economic and Social Affairs, Population Division*. Recuperado de: https://www.un.org/en/events/citiesday/assets/pdf/the_worlds_cities_in_2018_data_booklet.pdf

USGS. (2013). Landsat 8 (L8) Data Users Handbook | Landsat Missions (Vol. 8, Issue June). Recuperado de: https://landsat.usgs.gov/landsat-8-l8-data-users-handbook

Virmani, S. M., Sahrawat, K. L., and Burford, J. R. (1982). Physical and Chemical Properties of Vertisols and their Management. *Twelfth International Congress of Soil Science*, 80–93.

Weng, Q., Lu, D., and Schubring, J. (2004). Estimation of land surface temperature-vegetation abundance relationship for urban heat island studies. *Remote Sensing of Environment*, *89*, 467–483. https://doi.org/10.1016/j.rse.2003.11.005

Yu, X., Guo, X., and Wu, Z. (2014). Land surface temperature retrieval from landsat 8 TIRS-comparison between radiative transfer equation-based method, split window algorithm and single channel method. *Remote Sensing*, *6*, 9829–9852. https://doi.org/10.3390/rs6109829

Zhao-Liang, L., Bo-Hui, T., Hua, W., Huazhong, R., Guangjian, Y., Zhengming, W., Trigo, I. F., and Sobrino, J. (2013). Satellite-derived land surface temperature : Current status and perspectives. *Remote Sensing of Environment*, *131*, 14–37. https://doi.org/10.1016/j.rse.2012.12.008

Zhao-Liang, L., Hua, W., Ning, W., Shi, Q., Sobrino, J., Zhengming, W., Bo-hui, T., and Yan, G. (2013). Land surface emissivity retrieval from satellite data. *International Journal of Remote Sensing*, *34*(9), 3084–3127. https://doi.org/10.1080/01431161.2012.716540